BIOCHEMISTRY
including biophysical chemistry & molecular biology
Article

Biochemistry **2010,** *49,* 9413–9423 9413
DOI: 10.1021/bi101405y

Mechanistic Studies of Agmatine Deiminase from Multiple Bacterial Species†

Justin E. Jones,‡,§ Christina J. Dreyton,‡,§ Heather Flick,§ Corey P. Causey,§ and Paul R. Thompson*,‡,§

‡*Department of Chemistry, The Scripps Research Institute, Scripps Florida, 120 Scripps Way, Jupiter, Florida 33458, United States, and* §*Department of Chemistry and Biochemistry, University of South Carolina, 631 Sumter Street, Columbia, South Carolina 29208, United States*

Received August 31, 2010; Revised Manuscript Received September 28, 2010

ABSTRACT: One subfamily of guanidino group-modifying enzymes (GMEs) consists of the agmatine deiminases (AgDs). These enzymes catalyze the conversion of agmatine (decarboxylated arginine) to *N*-carbamoyl putrescine and ammonia. In plants, viruses, and bacteria, these enzymes are thought to be involved in energy production, biosynthesis of polyamines, and biofilm formation. In particular, we are interested in the role that this enzyme plays in pathogenic bacteria. Previously, we reported the initial kinetic characterization of the agmatine deiminase from *Helicobacter pylori* and described the synthesis and characterization the two most potent AgD inactivators. Herein, we have expanded our initial efforts to characterize the catalytic mechanisms of AgD from *H. pylori* as well as *Streptococcus mutans* and *Porphyromonas gingivalis*. Through the use of pH rate profiles, pK_a measurements of the active site cysteine, solvent isotope effects, and solvent viscosity effects, we have determined that the AgDs, like PADs 1 and 4, utilize a reverse protonation mechanism.

The guanidino group-modifying enzymes (GMEs) make up a large group of enzymes that catalyze a variety of reactions, including guanidinium hydrolysis and amidino group transfer (*1*). Family members include agmatine deiminase (AgD),[1] amidinotransferase (AT), dimethylarginine dimethylaminohydrolase (DDAH), L-arginine deiminase (ADI), and protein arginine deiminase (PAD) (*1*). These enzymes all contain an active site Cys that plays a critical role in nucleophilic catalysis; nucleophilic attack on the guanidinium carbon generates an *S*-alkyl thiouronium intermediate that can be either hydrolyzed to generate a ureido group or transferred to an acceptor nucleophile (*1*).

In recent years, numerous studies have suggested that the dysregulation of individual GME family members is associated with human disease or points to potential drug targets. Examples of the former include the gene encoding an AT in *Aphanizomenon ovalisporum*, a cyanobacterium, which is found in a genomic region that contains the genes encoding the enzymes thought to be responsible for the biosynthesis of cylindrospermopsin, a hepatotoxin. These data suggest that AT may play a role in the synthesis of this molecule (*2*); clindrospermopsin contains a guanidinium group that is thought to be generated via the actions of an AT. Another example is DDAH. This enzyme catalyzes the conversion of asymmetric dimethylarginine (ADMA) into citrulline. Dysregulated DDAH activity may contribute to the onset and progression of heart disease because ADMA acts as a competitive inhibitor of nitric oxide synthase, an enzyme that generates nitric oxide (NO), and is a key cellular messenger that regulates the cardiovascular system (*3*). Consistent with this possibility is the fact that the levels of ADMA are elevated in patients with heart disease (*3*, *4*). Also consistent with this notion is the fact that a DDAH knockout mouse exhibits the hallmark symptoms of heart disease (*5*).

Potential drug targets among GME family members include the ADI in *Giardia lamblia*, which is the parasite responsible for causing giardiasis (i.e., beaver fever). In this organism, ADI metabolizes arginine to generate energy in the form of ATP, and siRNA knockdown experiments indicate that this enzyme is critical for parasite survival (*6*). Bacterial ADIs are also being investigated as potential therapeutics for the treatment of cancer (*7*). For example, in a recent phase II study, patients with hepatocellular carcinoma were administered pegylated ADI (*Mycoplasma arginini*) and had a mean survival of 15.8 months; the estimated increase in survival time was 7.3 months (*7*). The PADs also represent potential drugs targets given the fact that their activity appears to be dysregulated in several human diseases, including cancer, multiple sclerosis, colitis, and rheumatoid arthritis (*8*).

In addition to the aforementioned GMEs, the AgDs, which catalyze the deimination of agmatine (i.e., decarboxylated arginine) to form *N*-carbamoyl putrescine (NCP) and ammonia (Figure 1), are potential drug targets. These enzymes are present in plants, bacteria, and viruses, where they are thought to play a role in energy generation, polyamine biosynthesis, and biofilm formation (*9*−*12*). In pathogenic bacteria (e.g., *Streptococcus mutans*, *Pseudomonas aeruginosa*, and *Helicobacter pylori*), these enzymes may also mediate acid resistance. However, in humans, agmatine is a cell signaling molecule involved in triggering a number of

†This work was supported in part by the University of South Carolina Research Foundation (P.R.T.), by The Scripps Research Institute of Scripps Florida, and in part by National Institutes of Health Grant GM079357 to P.R.T.

*To whom correspondence should be addressed: Department of Chemistry, The Scripps Research Institute, Scripps Florida, 130 Scripps Way, Jupiter, FL 33458. Telephone: (561) 228-2860. Fax: (561) 228-2918. E-mail: Pthompso@scripps.edu.

[1]Abbreviations: AgD, agmatine deiminase; NCP, *N*-carbamoyl putrescine; PAD, protein arginine deiminase; Cit, citrulline; BAEE, benzoyl L-arginine ethyl ester; BAA, benzoyl L-arginine amide; DTT, dithiothreitol; GST, glutathione *S*-transferase; TCEP, tris(2-carboxyethyl)phosphine hydrochloride; HEPES, *N*-(2-hydroxyethyl)piperazine-*N*′-2-ethanesulfonic acid; Orn, ornithine; ABFA, *N*-(4-aminobutyl)-2-fluoroethanimidamide; ABCA, *N*-(4-aminobutyl)-2-chloroethanimidamide.

Published on Web 09/28/2010

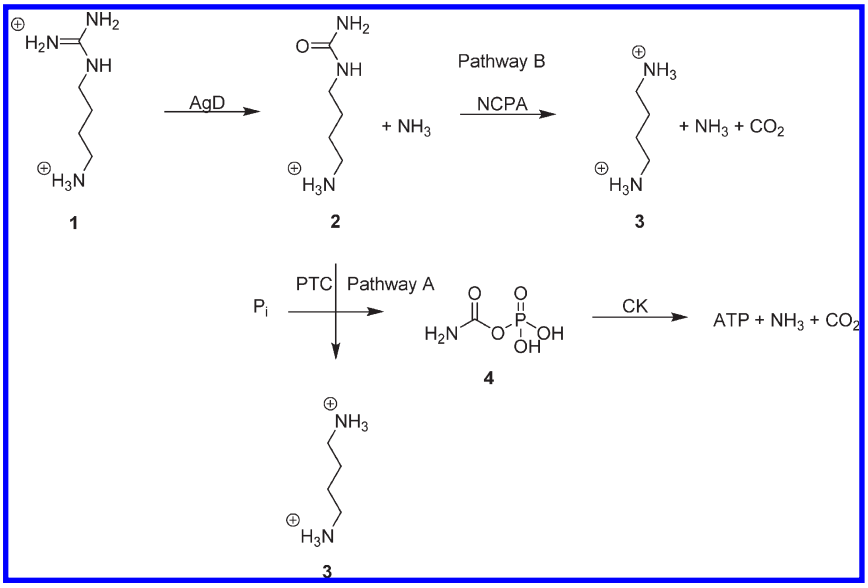

FIGURE 1: Agmatine metabolism in bacteria. In pathway A, agmatine, **1**, is converted to *N*-carbamoyl putrescine (NCP), **2**, and NH_3 by agmatine deiminase (AgD). For *S. mutans*, **2** is converted into putrescine, **3**, by putrescine transcarbamoylase (PTC). P_i reacts with carbamoyl to form carbamoyl phosphate, **4**, which is degraded to ATP, NH_3, and CO_2 by carbamate kinase (CK). In pathway B, for *H. pylori* and *Porphromonas gingivalis*, **2** is converted by NCP amidohydrolase (NCPA), to **3**, NH_3, and CO_2.

cellular processes (*13*−*17*), including the innate immune response. Thus, organisms that express agmatine-degrading enzymes possess a potential mechanism for evading this component of the human immune system. A similar role for *H. pylori* arginase has also been proposed; the depletion of arginine attenuates the innate immune response (*18*). Given these putative roles in disease, many laboratories have become focused on developing inhibitors and chemical probes targeting individual members of this family (*8*, *19*−*26*).

To gain insights into aiding inhibitor development, we and others initiated studies to characterize the catalytic mechanisms of a variety of GME family members, including a number of bacterial ADIs, DDAHs, as well as the PADs (*1*, *6*, *27*−*29*). Recently, we reported the purification, initial kinetic characterization, and structure of an AgD from *H. pylori*. Furthermore, site-directed mutagenesis verified that Cys324 is critical for catalysis and that Asp198 plays an important role in substrate recognition. Herein, we describe detailed mechanistic studies of the *H. pylori* enzyme (HpAgD), as well as AgDs from *S. mutans* (SmAgD), a Gram-positive bacterium, and *P. gingivalis* (PgAgD), a Gram-negative bacterium. Note that while PgAgD is classified in genomic databases as a putative PAD, we show here that it is in fact an AgD, similar to our previous studies establishing that the *H. pylori* enzyme is an AgD (*19*).

We chose to focus on AgDs from these three organisms because (i) each of these organisms contains an AgD, (ii) the enzymes are readily expressed (10−30 mg/L of medium), and (iii) all three enzymes are expressed by pathogenic bacteria that are responsible for a number of human ailments, including peptidic ulcers (*H. pylori*), tooth decay (*P. gingivalis*), and periodintitis and cardiovascular disease (*S. mutans*). In addition, these organisms metabolize agmatine differently. For example, *S. mutans* encodes a four-gene operon known as *agu*BDAC that metabolizes agmatine into putrescine, ATP, ammonia, and carbon dioxide (Figure 1). This system is thought to play a role in acid resistance and survival of the organism (*11*, *30*). On the other hand, *H. pylori* and *P. gingivalis* encode an AgD but do not contain the four-gene operon described above. Instead, these

Scheme 1: Inactivator Binding to E-SH (top) or E-S^- (bottom)

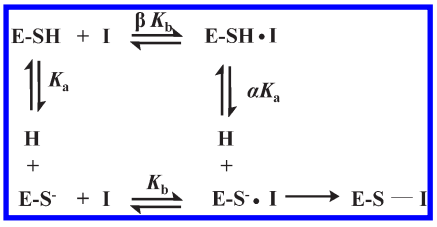

bacteria contain an AgD that converts agmatine to NCP, which is then hydrolyzed to putrescine, ammonia, and CO_2 via NCP amidohydrolase (Figure 1).

The active site architecture of the GME superfamily has been shown to be highly conserved, but the catalytic mechanisms vary between family members. For instance, PADs 1, 3, and 4 utilize reverse protonation mechanisms (*28*, *29*), while another enzyme in the same family, DDAH, has been suggested to use a substrate-assisted mechanism (*27*). In the latter mechanism, substrate binds to the thiol form of the enzyme and the positive charge of the guanidinium depresses the thiol pK_a such that the thiol proton is donated to solvent or an unknown base (Scheme 1, top pathway). In contrast, in a reverse protonation mechanism, substrate binds preferentially to the thiolate form of the enzyme (Scheme 1, bottom pathway). To improve our understanding of AgD catalysis and address whether these enzymes use a substrate-assisted or reverse protonation mechanism, we conducted detailed mechanistic studies of HpAgD, SmAgD, and PgAgD. Herein, we report the results of pH rate profiles, pK_a measurements on the active site thiol, solvent isotope effects (SIEs), and solvent viscosity effects (SVEs). The results indicate that, like other GME hydrolases (*1*, *6*, *27*−*29*), these enzymes possess a high-pK_a active site Cys, suggesting that these enzymes employ a reverse protonation mechanism. Furthermore, pK_a measurements with *N*-(4-aminobutyl)-2-fluoroethanimidamide (ABFA), a recently described AgD inhibitor (*19*), show that inactivation proceeds via a multistep mechanism that requires general acid catalysis.

MATERIALS AND METHODS

Chemicals. Iodoacetamide and 2-chloroacetamidine were purchased from Oakwood Products (Columbia, SC). Dideuterium oxide was obtained from Cambridge Isotope Laboratories (Andover, MA). Agmatine sulfate was purchased from Sigma-Aldrich (St. Louis, MO). ABFA and *N*-(4-aminobutyl)-2-chloroethanimidamide (ABCA) were synthesized as previously described (*19*).

Construction of an Expression Vector for SmAgD and PgAgD. *S. mutans* UA159 chromosomal DNA, which was the generous gift of R. A. Burne (University of Florida, Gainesville, FL), was used to amplify the SmAgD gene by PCR with the following primers: 5′-AAAAAACATATGGCAAAACGTATTAAAAATACAACTCC-3′ and 5′-AAAAAACTCGAGTTAAGTTGCAGGTTGCTGTTGTGTAATACAG-3′. The forward primer contains an *Nde*I restriction site (underlined) followed by 26 bases that correspond to the 5′-coding region of the SmAgD gene. The reverse primer contains an *Xho*I restriction site (underlined) followed by 31 bases that correspond to the 3′-coding region of SmAgD. The PCR-amplified gene was then treated with *Nde*I and *Xho*I to facilitate cloning into the pET21 vector. The resulting pET21SmAgD construct was sequenced to ensure that no mutations were incorporated during the PCR amplification.

P. gingivalis W83 chromosomal DNA, which was obtained from M. E. Davey (The Forsyth Institute, Boston, MA), was used as the template to PCR amplify the gene encoding PgAgD with the following primers: 5′-AAAAAACATATGACAAAGAGACTATTCCTGCCCGAATGGGC-3′ and 5′-AAAAAACTCGAGTTAGCGTATGAATCCTTGGGGG-3′. The forward primer contains an *Nde*I restriction site (underlined) followed by 29 bases that correspond to the 5′-coding region of the PgAgD gene. The reverse primer contains an *Xho*I restriction site (underlined) followed by 22 bases that correspond to the 3′-coding region of PgAgD. The PCR-amplified gene was then treated with *Nde*I and *Xho*I to facilitate cloning of the PgAgD gene into the pET21 vector. The resulting pET21PgAgD construct was sequenced to ensure that no mutations were incorporated during the PCR amplification.

Purification of HpAgD, SmAgD, and PgAgD. Both the *S. mutans* and *P. gingivalis* AgD enzymes were purified in a manner analogous to the method previously described for HpAgD (*19*). Briefly, the protein was recombinantly expressed, lysed by sonication, and then purified by a combination of anion exchange, heparin affinity, and size exclusion chromatography. The protein was ≥95% pure as assessed by sodium dodecyl sulfate−polyacrylamide gel electrophoresis (SDS−PAGE). The protein was stored at −80 °C and was stable for ≥6 months.

Kinetic Assay. A discontinuous assay that measures ureido-containing compounds was used to measure HpAgD, SmAgD, and PgAgD activity (*31*, *32*). Briefly, ureido groups produced during the reaction (i.e., NCP) react with diacetyl monooxime under strongly acidic conditions to generate a chromophore that absorbs at 540 nm. Comparison of these absorbance values to a standard curve was used to quantify NCP product formation. The steady state kinetic parameters were determined by preincubating varying amounts of agmatine in 50 mM 4-(2-hydroxyethyl)-1-piperazineethanesulfonic acid (HEPES) (pH 8.0) in a final volume of 60 μL prior to the addition of enzyme to initiate the reaction. Reactions were allowed to proceed for either 10 min (HpAgD and PgAgD) or 6 min (SmAgD) at 37 °C. Enzyme activity was linear with respect to both time and enzyme concentration. Standard errors were typically less than 20%. Initial rates were fit by nonlinear least-squares fit to eq 1

$$v = V_{max}[S]/(K_m + [S]) \quad (1)$$

using GraFit version 5.0.11 (*33*).

pH Studies. pH profiles were generated for HpAgD, PgAgD, and SmAgD by measuring the initial rates over a range of pH values (5.5−9.5) in 50 mM 2-[bis(2-hydroxyethyl)amino]-2-(hydroxymethyl)propane-1,3-diol (Bis-Tris) (pH 5.5−7.0), HEPES (pH 7.0−8.75), and *N*-cyclohexyl-2-aminoethanesulfonic acid (CHES) (pH 8.75−9.5) in the presence of various concentrations of agmatine (0−5 mM). The initial rates were fit to eq 1, and the k_{cat} and k_{cat}/K_m values obtained for each pH value were then plotted versus pH and fit to either eq 2 for PgAgD and SmAgD or eq 3 for HpAgD (k_{cat} data only)

$$y = Y_{max} - \log(1 + K_2/K_1 + H/K_1 + K_2/H) \quad (2)$$

$$y = Y_{max} + \log(1 + H/K_2) - \log(1 + H/K_1) \quad (3)$$

using GraFit version 5.0.11 (*33*). Y_{max} corresponds to the activity at the pH optimum. Note that an overlapping buffer scheme was used to ensure that alterations in the kinetics are not due to buffer effects. Specifically, k_{cat} and k_{cat}/K_m values were determined at pH 7.0 and 8.75 in two different buffers, and the data were averaged; the values were in agreement between the two buffers. Also note that at each of the pH values tested, time course experiments were performed and were linear for ≥15 min. For these experiments, buffer and substrate were preincubated for 10 min and the reaction was initiated by the addition of enzyme. Aliquots were taken at 0, 2, 4, 6, 10, and 15 min, and the reaction was quenched when the mixture was flash-frozen in liquid nitrogen. Product formation was assessed as described above.

Iodoacetamide Inactivation Experiments. For SmAgD, 2 μM enzyme was incubated at 37 °C with an inactivation mix containing 50 mM HEPES (pH 7.0−9.0) and varying concentrations of iodoacetamide (0−20 mM). At different time points from 0 to 30 min, aliquots were removed from the inactivation mix and subsequently added to a reaction mix [50 mM HEPES (pH 8), 5 mM β-mercaptoethanol (to quench the iodoacetamide), and 5 mM agmatine] to measure residual AgD activity. This reaction proceeded for 15 min and was quenched in liquid nitrogen. Product formation was then quantified using the methodology outlined above. For each iodoacetamide concentration, data were fit to eq 4

$$v = v_o e^{-kt} \quad (4)$$

using GraFit version 5.0.11 (*33*). v is the velocity, v_o the initial velocity, k the pseudo-first-order rate constant (i.e., k_{obs}), and t the time. Plots of the observed inactivation rates (k_{obs}) versus inactivator concentration were linear and fit to eq 5

$$k_{obs} = (k_{inact}/K_I)[I] \quad (5)$$

where k_{inact} is the maximal inactivation rate, K_I is the concentration that yields half-maximal inactivation, and [I] is the concentration of inactivator. The slopes of these plots, which correspond to k_{inact}/K_I, were then plotted versus pH and fit to eq 6

$$y = [(Y_{min} + Y_{max}) \times 10^{pH - pK_a}]/(10^{pH - pK_a} + 1) \quad (6)$$

using GraFit version 5.0.11. Y_{min} and Y_{max} correspond to the minimum and maximum rates of inactivation, respectively.

For HpAgD, time course experiments in the absence and presence of increasing concentrations of iodoacetamide were performed over a range of pH values (pH 7.50−9.25). For these assays, 0.5 mM agmatine (dissolved in 50 mM HEPES) was incubated with various concentrations of iodoacetamide (0−20 mM) for 10 min at 37 °C. Subsequently, HpAgD was added to initiate the reaction. Aliquots (60 μL) were taken at different time points (0, 2, 4, 6, 8, 10, 15, and 20 min) and the reactions quenched when the mixtures were flash-frozen in liquid nitrogen. NCP production was quantified using the methodology outlined above and plotted versus time. The data were subsequently fit to eq 7

$$[P] = v_i[1 - \exp^{-k_{obs(app)}t}]/k_{obs(app)} \quad (7)$$

using GraFit version 5.0.11. *P* corresponds to the quantity of NCP produced during the reaction. v_i is the initial velocity. $k_{obs(app)}$ is the apparent pseudo-first-order rate constant for enzyme inactivation. *t* corresponds to time. To obtain k_{obs} values, the $k_{obs(app)}$ values were subsequently extrapolated to zero substrate concentration using the transformation described by eq 8

$$1 + [S]/K_m \quad (8)$$

The second-order rate constants for the inactivation of HpAgD by iodoacetamide, i.e., k_{inact}/K_I, were then determined by plotting k_{obs} versus iodoacetamide concentration and fitting the data to eq 5 using Grafit version 5.0.11. The slopes of these plots, which correspond to k_{inact}/K_I, were then plotted versus pH and fit to eq 6.

2-Chloroacetamidine Inactivation Experiments. The 2-chloroacetamidine inactivation experiments were performed essentially as described above. For SmAgD, inactivation mixtures, containing 50 mM HEPES (pH 7.0−9.0), were incubated with 2 μM SmAgD for 10 min at 37 °C. Various concentrations of 2- chloroacetamidine (0−1 mM) were then added, and aliquots at various time points (0−30 min) were removed and added to reaction mix containing 5 mM agmatine. The data were processed as described above.

For HpAgD, various concentrations of 2-chloroacetamidine (0−60 mM) were preincubated with 0.5 mM agmatine in 50 mM HEPES (pH 7.50−9.25) for 10 min at 37 °C. Reactions were then initiated by the addition of HpAgD and 60 μL aliquots taken at different time points (0, 2, 4, 6, 8, 10, 15, and 20 min). Reactions were quenched when the mixtures were flash-frozen in liquid nitrogen. NCP levels were quantified using the methodology outlined above, and the pseudo-first-order rate constants for enzyme inactivation were determined. Because saturation was observed in the plots of k_{obs} versus [I], the data were fit to eq 9

$$k_{obs} = k_{inact}[I]/(K_I + [I]) \quad (9)$$

using GraFit version 5.0.11. k_{inact} corresponds to the maximal rate of inactivation, and K_I is the concentration of I that yields half-maximal inactivation. k_{inact}/K_I was then plotted versus pH and fit to eq 6.

Substrate Protection. To evaluate the ability of substrate to protect against iodoacetamide- and 2-chloroacetamidine-induced inactivation, progress curves were generated with and without inactivator (50 mM iodoacetamide or 2-chloroacetamidine) at two different concentrations of substrate. For iodoacetamide, agmatine concentrations of 0.25 mM (8K_m for HpAgD and 2K_m for SmAgD) and 5 mM (170K_m for HpAgD and 13K_m for SmAgD) were used. For 2-chloroacetamidine, agmatine concentrations of 0.5 mM (17K_m for HpAgD and 2K_m for SmAgD) and 2 mM (67K_m for HpAgD and 5K_m for SmAgD) were used. Assay buffer was preincubated for 10 min at 37 °C, and either HpAgD or SmAgD was added to initiate the reaction. Aliquots (60 μL) were taken at 0, 2, 4, 6, and 10 min, and data analysis was performed as described above.

ABFA Inactivation. ABFA inactivation experiments were performed using the methodology outlined above for the iodoacetamide and 2-chloroacetamide inactivation experiments. Briefly, various concentrations of ABFA (0−1 mM) were preincubated with 0.5 mM agmatine in 50 mM HEPES (pH 7.0−9.0) for 10 min at 37 °C. Reactions were then initiated by the addition of SmAgD, and aliquots (60 μL) were removed at specific time points (0, 1, 2, 3, 4, 5, and 6 min). Reactions were quenched when the mixtures were flash-frozen in liquid nitrogen. NCP levels were quantified using the methodology outlined above, and the apparent pseudo-first-order rate constants for enzyme inactivation were determined. Saturation was observed only at the pH optimum (pH 8), and the k_{obs} versus [I] data were fit to eq 8 using GraFit version 5.0.11. For all other pH values, the data were fit to eq 5. k_{inact}/K_I was then plotted versus pH and fit to eq 6.

Solvent Isotope and Solvent Viscosity Effects. All buffers and solutions were prepared in D_2O. Buffer pD values were determined using the formula pD = pH + 0.4. Reactions were performed in 50 mM Bis-Tris (pL 6.0−6.5), Tris (pL 7.0−8.5), and CHES (pL 8.5) in the presence of various concentrations of agmatine (0.0−2.5 mM) in >95% D_2O. Reactions were performed and analyzed as described above. Solvent viscosity experiments were performed in 50 mM HEPES (pH 8.0) and various concentrations of agmatine (0.0−2.5 mM) in 0, 10, 20, 25, and 30% glycerol. The relative viscosity was measured using a Cannon Manning Semi-Micro Viscometer size 50 (Cannon Instrument Co.). Data analyses were performed as described above.

IC_{50} Determination. The IC_{50} values of ABFA and ABCA were determined for SmAgD and PgAgD as previously described (*19*). Varying concentrations of inhibitor were preincubated with enzyme in 50 mM HEPES (pH 8) for 15 min at 37 °C. Agmatine (0.5 mM) was added and allowed to react for 15 min. The reaction was quenched when the mixture was flash-frozen in liquid nitrogen, and product was measured as described above. Rates were fit to eq 10

$$\text{fraction activity} = 1/(1 + [I]/IC_{50}) \quad (10)$$

using GraFit version 5.0.11 (*33*), where [I] is the inhibitor concentration and IC_{50} is the concentration of inhibitor that yields half-maximal activity.

RESULTS

pH Studies. In an effort to identify the optimal pH for AgD activity, as well as to begin to characterize the catalytic mechanism of these enzymes, pH profiles were constructed for HpAgD, SmAgD, and PgAgD by determining the steady state kinetic parameters of agmatine deimination over a range of pH values (5.0−10.0). The plots of log k_{cat}/K_m versus pH (Figure 2) are bell-shaped for all three enzymes, suggesting that two ionizable groups, with pK_a values of 7.9 ± 0.4 and 8.1 ± 0.4 for HpAgD, 6.8 ± 0.2 and 9.4 ± 0.3 for PgAgD, and 6.1 ± 0.2 and 9.2 ± 0.3 for SmAgD, contribute to substrate capture; effects on substrate capture include all steps (both substrate binding and transition state formation) up to and including the first irreversible step of the reaction. Note that deiminase activity was linear with respect to

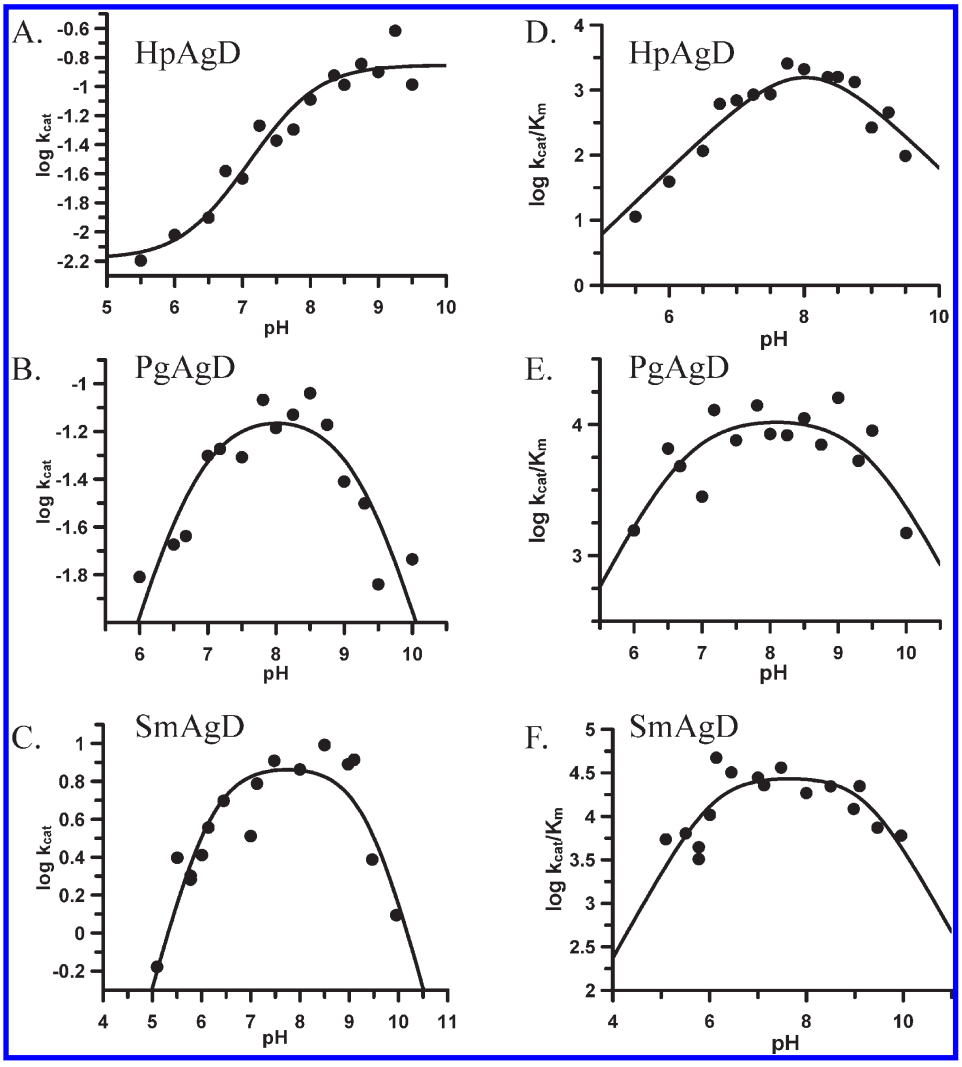

FIGURE 2: Log k_{cat} vs pH rate profiles for (A) HpAgD, (B) PgAgD, and (C) SmAgD. Log k_{cat}/K_m vs pH rate profiles for (D) HpAgD, (E) PgAgD, and (F) SmAgD.

time over the entire pH range studied, thereby indicating that the loss of activity is not due to a nonspecific effect on enzyme stability.

The plots of log k_{cat} versus pH were also bell-shaped for PgAgD and SmAgD with a pH optimum of ~8.0 (Figure 2), suggesting that two ionizable groups contribute to the rate-limiting step of the reaction. The pK_a values obtained from this analysis are 6.8 ± 0.2 and 9.2 ± 0.2 for PgAgD and 6.1 ± 0.1 and 9.4 ± 0.2 for SmAgD. In contrast to PgAgD and SmAgD, the plot of log k_{cat} versus pH for HpAgD fits well to a model in which only one ionizable group contributes to the rate-limiting step (pK_a = 7.2 ± 0.2, and slope = 0.7 ± 0.2).

Solvent Isotope Effects. pD profiles were also generated by measuring the steady state kinetic parameters in >95% D_2O. For HpAgD, plots of pL versus log k_{cat}/K_m and log k_{cat} in H_2O and D_2O are bell-shaped and sigmoidal, respectively (Figure 3). The solvent isotope effects (SIEs) were also examined for HpAgD and SmAgD at the pH optimum. The results indicate that with respect to k_{cat}/K_m the reaction rate is faster in D_2O for both enzymes [$(k_{cat}/K_m^{H})/(k_{cat}/K_m^{D})$ = 0.71 ± 0.30 for HpAgD, and $(k_{cat}/K_m^{H})/(k_{cat}/K_m^{D})$ = 0.44 ± 0.11 for SmAgD]. With respect to k_{cat}, an inverse SIE was observed for HpAgD, whereas for SmAgD, the SIE was normal. The SIE values are as follows: k_{cat}^{H}/k_{cat}^{D} = 0.62 and k_{cat}^{H}/k_{cat}^{D} = 1.05 for HpAgD and SmAgD, respectively.

Such inverse SIEs can be caused by medium effects, the dissociation of a metal-chelated water, viscosity effects, or effects on thiol ionization (*34*). Although we cannot exclude effects of the medium as a possible cause of the inverse SIE, these are typically small and normally discounted (*34*). Additionally, given that there are no metal ions required for catalysis and the viscosity effect is near zero (see below), the inverse SIE is most likely due to effects on thiol ionization; the fractionation factor of a thiol in D_2O is ~0.5, which results in an increased concentration of the thiolate species in D_2O (*35*). Given that the magnitude of these inverse SIEs on k_{cat}/K_m is similar to the fractionation factor of a thiol in D_2O, these data suggest that the enhanced reactivity of HpAgD and SmAgD in D_2O is due to the higher concentration of the reactive thiolate, i.e., an equilibrium SIE. Similar inverse SIEs on k_{cat}/K_m have been observed for other guanidinium-modifying enzymes, e.g., PADs 1 and 4 (*28*, *29*), as well as other thiol-containing enzymes, e.g., papain (*36*).

Solvent Viscosity. Solvent viscosity experiments were also performed to aid the characterization of AgD catalysis. For these experiments, the steady state kinetic parameters were measured in assay buffers containing various concentrations of glycerol. The slopes obtained from plots of relative viscosity versus relative k_{cat}/K_m or relative k_{cat} are near zero for all of the enzymes tested (Table 1; see Figure 4 for representative data obtained with

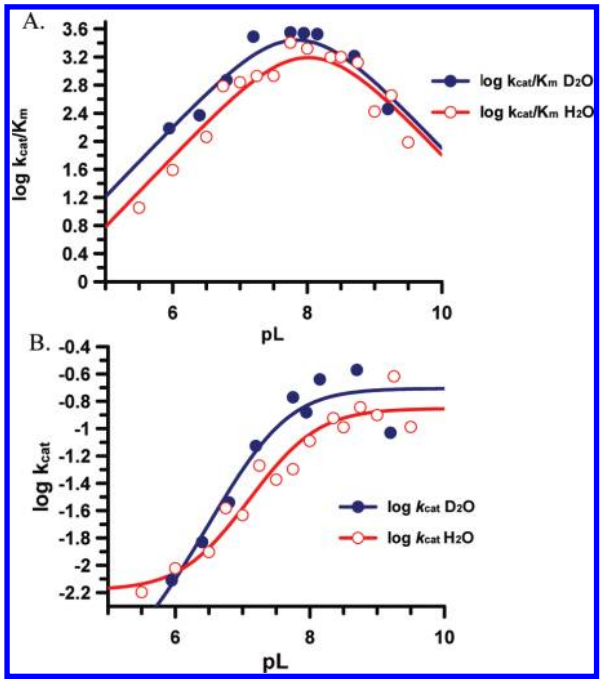

FIGURE 3: Solvent isotope effect for HpAgD. (A) Plot of log k_{cat}/K_m vs pH in H_2O (red) and D_2O (blue). (B) Plot of log k_{cat} vs pH in H_2O (red) and D_2O (blue).

Table 1: Solvent Viscosity Effect

	SmAgD	HpAgD
slope of relative viscosity vs relative k_{cat}	0.22 ± 0.20	-0.08 ± 0.10
slope of relative viscosity vs relative k_{cat}/K_m	-0.12 ± 0.14	-0.12 ± 0.06

HpAgD). This lack of a solvent viscosity effect on k_{cat} and k_{cat}/K_m indicates that product release and substrate binding, respectively, are not rate-limiting.

Iodoacetamide Inactivation Kinetics. To determine the pK_a of the active site cysteine in HpAgD and SmAgD, the rates of iodoacetamide-induced enzyme inactivation were determined as a function of time over a pH range of 7.0−9.25 (little to no inactivation was observed at lower pH values). For HpAgD, product formation was plotted versus time and then fit to a single-exponential decay to determine the pseudo-first-order rate constants of iodoacetamide inactivation, i.e., k_{obs} (Figure 5). For SmAgD, the k_{obs} was determined by generating progress curves in the absence and presence of increasing concentrations of iodoacetamide (not shown). The second-order rate constants for iodoacetamide inactivation, i.e., k_{inact}/K_I, were then obtained from the slopes of the plots of k_{obs} versus iodoacetamide concentration (Figure 5C). This process was repeated over the entire pH range, and the k_{inact}/K_I values were plotted as a function of pH. As depicted in Figure 6, k_{inact}/K_I increases with pH and fits to eq 6 are consistent with a single ionizable group with a pK_a of 9.2 ± 0.3 for HpAgD and 9.6 ± 0.3 for SmAgD. Given that the pK_a values are so high, it was not technically feasible to observe a plateau in the titration curves. Therefore, these values should be considered lower limits. Nevertheless, these data along with the pH profiles indicate that both HpAgD and SmAgD, like other guanidinium-modifying enzymes (*6*, *27*−*29*), possess a high-pK_a active site thiol. Note that substrate protection experiments are

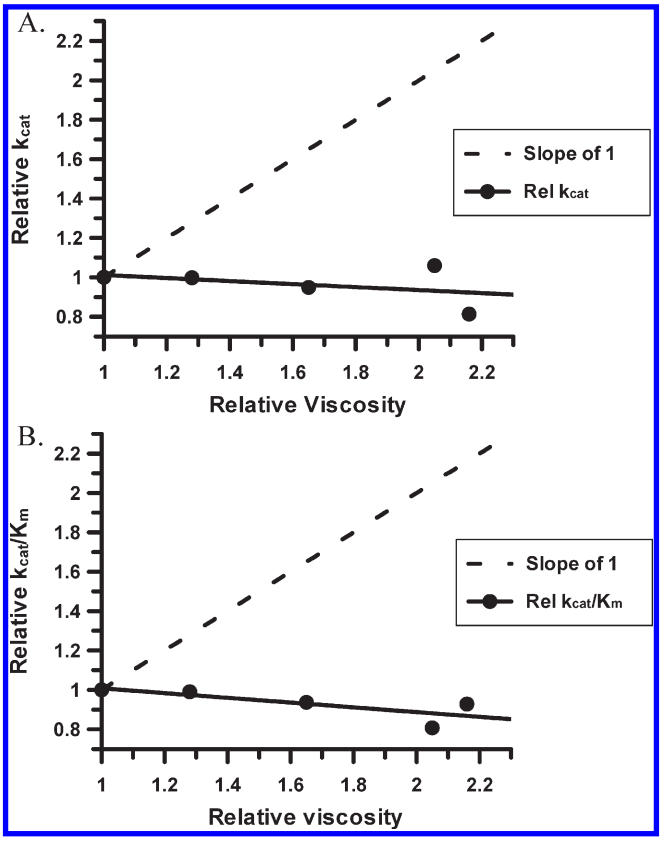

FIGURE 4: Solvent viscosity effect for HpAgD. (A) Plot of relative viscosity vs relative k_{cat}. (B) Plot of relative viscosity vs relative k_{cat}/K_m.

consistent with the modification of an active site residue (Figure 5A).

2-Chloroacetamidine Inactivation Kinetics. pK_a measurements with 2-chloroacetamidine were also performed to evaluate whether the positively charged nature of this compound could depress the pK_a of the active site cysteine by mimicking the effect of the positively charged guanidinium group in agmatine. Inactivation experiments were performed in a manner analogous to those described above for iodoacetamide. Representative plots of product formation versus time are depicted in Figure 7 for HpAgD. For HpAgD, plots of k_{obs} versus 2-chloroacetamidine concentration were hyperbolic (Figure 7C), thereby suggesting saturatable kinetics. k_{inact}/K_I values were obtained by fitting the observed data to eq 9. Subsequent plots of k_{inact}/K_I versus pH and k_{inact} versus pH were then generated by repeating these experiments over the entire pH range. As depicted in Figure 8, k_{inact}/K_I increases as a function of pH and suggests that the pK_a value of Cys324 in the free enzyme is 9.8 ± 0.1. This value is in reasonable agreement with the descending limb of the pH versus k_{cat}/K_m rate profiles. k_{inact} also increases as a function of pH and displays a pK_a of 9.3 ± 0.5 (Figure 8C). For SmAgD, plots of residual activity versus 2-chloroacetamide concentration were linear over the range of 2-chloroacetamidine concentrations tested. Plots of k_{inact}/K_I versus pH were then generated by performing the same experiments described above over the entire pH range, and a pK_a value of 8.8 ± 0.1 was determined (Figure 8C). This value is also in reasonable agreement with the pK_a corresponding to the descending limb of the pH versus k_{cat}/K_m rate profile (i.e., 9.2 ± 0.3). The data for both HpAgD and SmAgD indicate that the positive charge of the inactivation does not depress the pK_a of the active site thiol to an appreciable extent. Note that

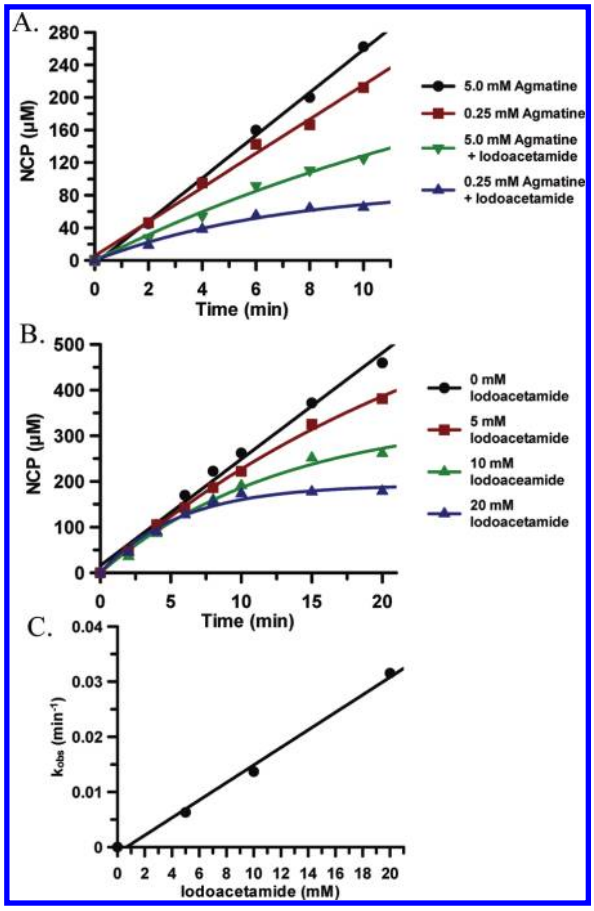

FIGURE 5: Iodoacetamide inactivation experiments for HpAgD. (A) Substrate protection experiment. (B) Progress curves with increasing concentrations of iodoacetamide. (C) Plot of k_{obs} vs iodoacetamide concentration.

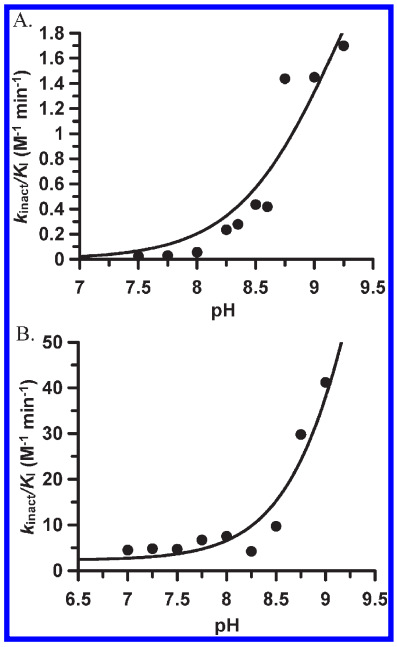

FIGURE 6: k_{inact}/K_I values obtained from iodoacetamide inactivation experiments plotted vs pH for HpAgD (A) and SmAgD (B).

substrate protection experiments were performed to ensure that the inactivation was due to the modification of an active site residue (see Figure 7A for representative data obtained with HpAgD).

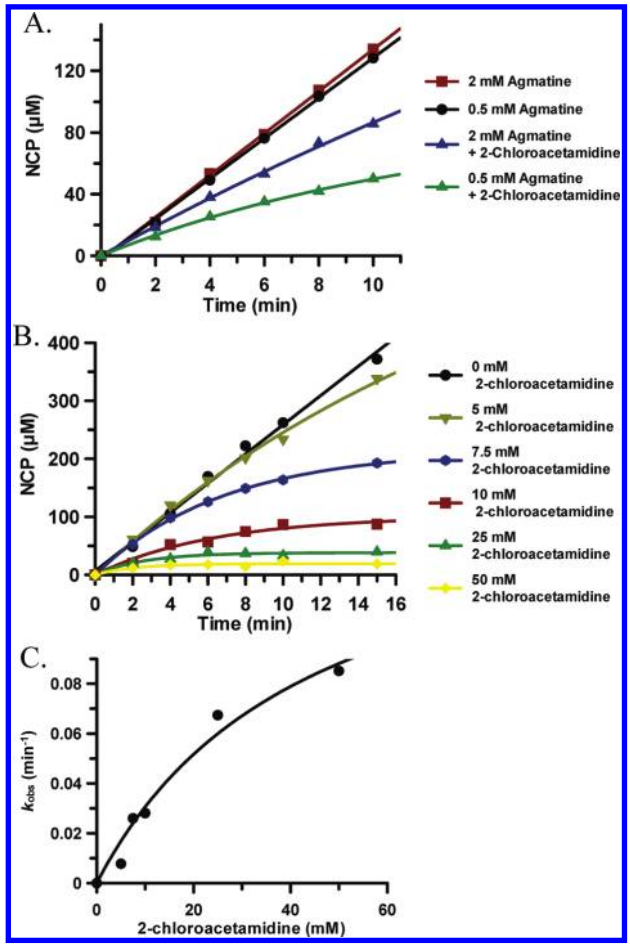

FIGURE 7: 2-Chloroacetamidine inactivation experiments. (A) Substrate protection experiment for HpAgD. (B) Progress curves with increasing concentrations of 2-chloroacetamidine. (C) Plot of k_{obs} vs 2-chloroacetamidine concentration.

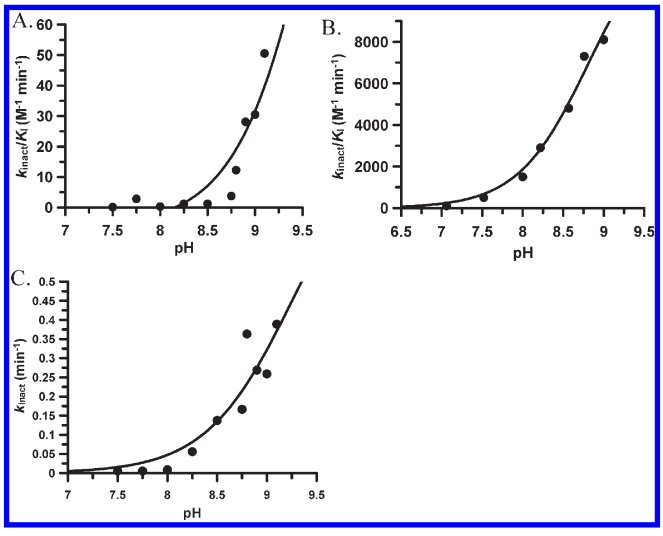

FIGURE 8: pH dependence of 2-chloroacetamidine inactivation. (A) Plot of k_{inact}/K_I vs pH obtained with HpAgD. (B) Plot of k_{inact} vs pH obtained with HpAgD. (C) Plot of k_{inact}/K_I vs pH obtained with SmAgD.

IC_{50} Data with SmAgD and PgAgD. Previously, we reported that ABFA and ABCA (IC_{50} = 6.8 and 0.87 μM, respectively) are potent, mechanism-based inactivators of HpAgD that covalently modify the active site thiolate, i.e., Cys324 (*19*). To determine if ABFA and ABCA inhibit all the

AgDs, we measured IC_{50} values for SmAgD and PgAgD (Table 2). Although the IC_{50} values for SmAgD are significantly more potent than those obtained for either HpAgD or PgAgD, these results indicate that ABFA and ABCA are *pan* AgD inhibitors.

ABFA Inhibition Experiments with SmAgD. ABFA and ABCA likely inactivate the AgDs through one of at least two possible mechanisms (Figure 9A,B). The first mechanism involves the simple displacement of the halide in a S_N2 manner. In the second mechanism, the active site thiolate attacks the iminium carbon, forming a tetrahedral intermediate. The sulfur then displaces the halide to form a three-member sulfonium ring, which collapses to form the inactivated thioether. To characterize the mechanism by which ABFA inactivates SmAgD, we determined the rates of inactivation for SmAgD as a function of pH. Note that these studies focused only on SmAgD because this enzyme displays rates of catalysis significantly higher than those of either HpAgD or PgAgD and is thus better behaved. As seen in Figure 10, the plots of k_{inact}/K_I versus pH are bell-shaped, suggesting that two ionizable groups are critical for inactivator capture. Unfortunately, inactivator saturation was observed only at the pH optimum, and k_{inact} versus pH rate profiles could not be generated. Nevertheless, the data are consistent with data obtained for the fluoro- and chloroamidine-induced inactivation of PAD4; i.e., the k_{inact}/K_I versus pH rate profiles are also bell-shaped (*37*). On the basis of additional SIE, proton inventory, and k_{inact} versus pH rate profiles, these data indicated that general acid catalysis plays a critical role in the inactivation of PAD4 and further suggested that proton donation stabilizes the tetrahedral intermediate to facilitate the intramolecular displacement of the halide (Figure 9C). Given the similarities in the k_{inact}/K_I pH rate profiles, ABFA likely inactivates SmAgD via a similar mechanism.

Table 2: Summary of IC_{50} Values

inhibitor	IC_{50} for HpAgD (μM)	IC_{50} for SmAgD (μM)	IC_{50} for PgAgD (μM)
ABFA	6.8 ± 0.26	0.27 ± 0.10	91 ± 25
ABCA	0.87 ± 0.03	0.26 ± 0.61	15 ± 3

DISCUSSION

Numerous GME family members are associated with human disease and/or represent potential therapeutic targets for giardiasis (e.g., ADI), bacterial infections (e.g., ADIs and AgDs), and cancer, RA, and colitis (e.g., PADs). To gain insights into the common features, and potential differences, in the catalytic mechanisms of the GME hydrolases that could be used to aid inhibitor development, we and others have examined the catalytic

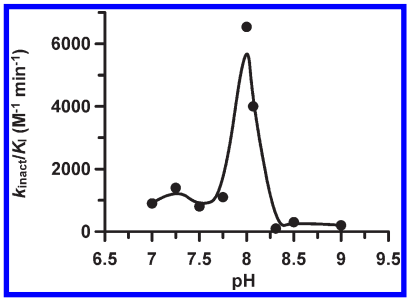

FIGURE 10: ABFA inactivation kinetics. Plot of k_{inact}/K_I vs pH for ABFA obtained with SmAgD.

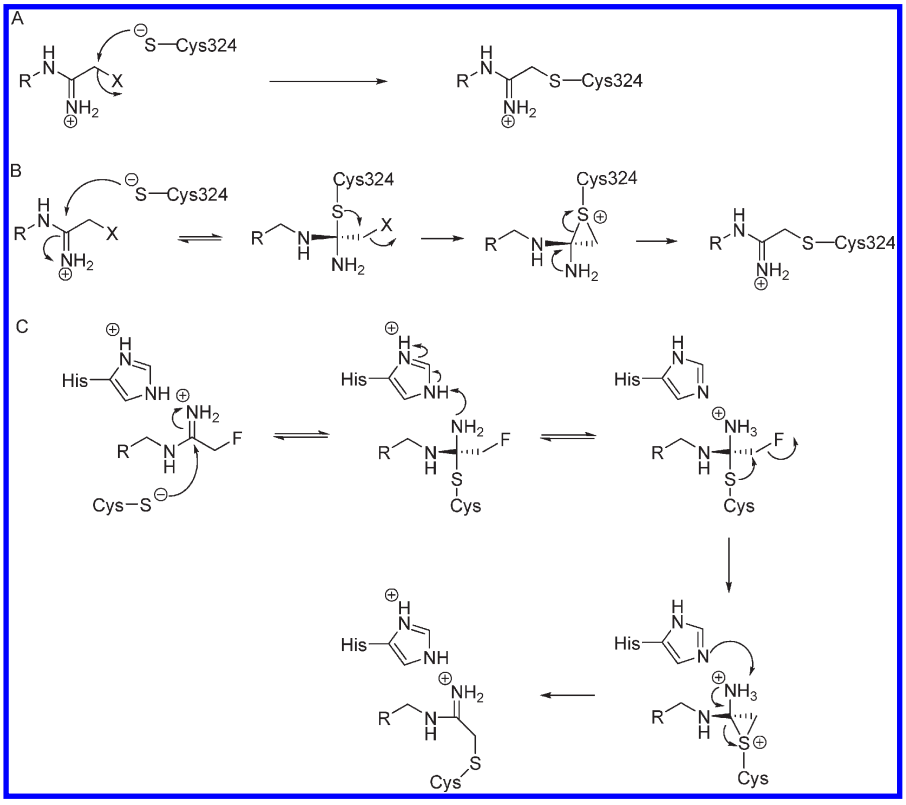

FIGURE 9: Three possible mechanisms of inactivation for ABFA and ABCA. (A) S_N2 displacement of the halide. (B) Multistep mechanism in which the active site thiolate attacks the imminium carbon to form a tetrahedral intermendiate. This intermediate rearranges to form a three-member sulfonium ring, which collapses to form the inactivated thioether moiety. (C) Multistep mechanism involving general acid catalysis to stabilize the initial tetrahedral intermediate.

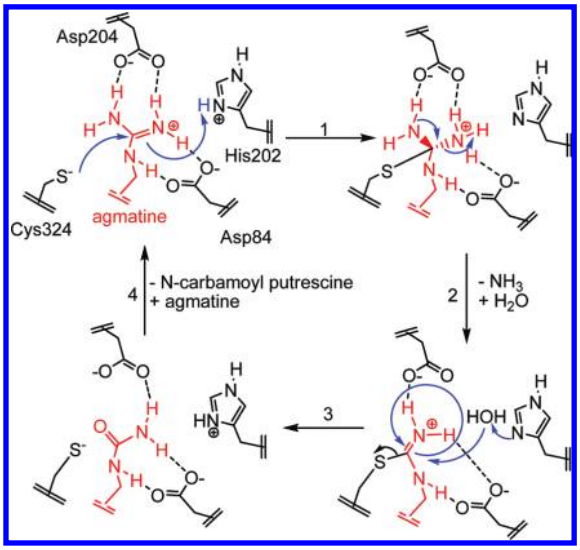

FIGURE 11: Mechanism of AgD catalysis (HpAgD numbering). The active site thiolate attacks the guanidinium carbon, and the histidine acts as a general acid to donate a proton to the departing amine. The tetrahedral intermediate collapses to form the *S*-alkylthiouronium intermediate. Ammonia is exchanged for a molecule of water, and the histidine acts as a general base, which activates the water molecule for nucleophilic attack. The second tetrahedral intermediate collapses to form the final product.

mechanism of several PADs, DDAHs, ADIs, and AgDs (*6*, *27*−*29*, *38*). On the basis of these studies, a generally accepted catalytic mechanism has been proposed. In this mechanism, Asp84 and Asp204 likely play critical roles in binding and orienting the substrate guanidinium for nucleophilic attack by the side chain thiolate of Cys324 (Figure 11, HpAgD numbering). His202 would then be expected to act as a general acid, donating a proton to the departing amine either during the initial formation of the developing tetrahedral intermediate or after its collapse. His202 would then switch roles and act as a general base to activate a water molecule for nucleophilic attack and subsequent hydrolysis of the thiouronium intermediate generated in the previous step. Several aspects of this mechanism have been verified, including the existence of the thiouronium intermediate in ADI and DDAH, as well as the key roles that the Asp groups, His, and Cys play in substrate recognition and activation, general acid−base catalysis, and covalent catalysis, respectively (*6*, *27*, *38*).

One issue regarding the mechanism that has drawn considerable debate is the protonation state of the active site Cys prior to substrate binding and how to reconcile the high pK_a of the thiol (*27*−*29*, *39*, *40*). Specifically, Fast and colleagues have suggested that DDAH utilizes a substrate-assisted mechanism; the substrate binds to the thiol form of the enzyme, and the positive charge of the guanidinium depresses the thiol pK_a such that the thiol proton is donated to solvent or an unknown base (Scheme 1). It is undoubtedly true that once bound, the proximity of the guanidinium to the thiol would decrease its pK_a by ≥2.8 pH units, as Fast and colleagues have shown using a reversible DDAH substrate analogue (*27*). However, it is unclear whether this mechanism is universally used by all GME hydrolases and/or whether it is the kinetically preferred pathway. Along those lines, we have suggested that the PADs utilize a reverse protonation mechanism, in which only a small amount of the enzyme exists as the nucleophilic thiolate and that substrate binds preferentially, but not exclusively, to the thiolate form of the enzyme (*28*, *29*).

To both further our understanding of GME hydrolase catalysis and guide the design of inhibitors targeting the AgDs, we set out to characterize the mechanism of AgD catalysis. The HpAgD, SmAgD, and PgAgD k_{cat}/K_m pH profiles are bell-shaped, indicating that there are two ionizable residues that are important for substrate capture. For SmAgD and PgAgD, the k_{cat} versus pH profiles are also bell-shaped, suggesting that two ionizable groups must be correctly protonated to achieve the maximum rate of hydrolysis. On the basis of precedents, these two ionizable groups likely correspond to the active site His and Cys (*27*, *28*). Surprisingly, the k_{cat} versus pH profile for HpAgD is sigmoidal. These data indicate that only one proton transfer event is rate-limiting for this enzyme and could suggest either that the catalytic mechanism used by HpAgD is different from the one utilized by SmAgD and PgAgD or, more likely, that the rate-limiting steps of the reaction differ between these enzymes. Given that HpAgD also exhibits an inverse SIE on k_{cat}, but no solvent viscosity effect, the simplest interpretation of the data is that nucleophilic attack on the substrate guanidinium is rate-limiting for HpAgD, but not for SmAgD or PgAgD.

To determine whether the Cys or the His corresponds to the ascending or descending limbs of the pH rate profiles, pK_a measurements were performed on the active site thiolate. This was accomplished by measuring the rate of inactivation of HpAgD and SmAgD over a range of pH values with iodoacetamide. On the basis of these experiments, the pK_a values of the active site Cys residue in HpAgD and SmAgD are 9.2 and 9.6, respectively, thereby suggesting that the pK_a of this Cys residue corresponds to the descending limb of the k_{cat}/K_m versus pH profile. As such, the ascending limb of the k_{cat}/K_m versus pH profile likely corresponds to the protonation state of the His. Given that these pK_a assignments are the reverse of the simplest assumption, i.e., that the rate of the reaction would increase as the thiolate concentration is increased, these data suggest that the AgDs, like the PADs, utilize what is commonly termed a reverse protonation mechanism; the term reverse protonation is used because it is the reverse of the simplest assumption (*41*, *42*). In such a mechanism, only a small fraction of the enzyme exists in the correct protonation state, i.e., the thiolate form, at the pH optimum (*28*, *29*, *41*, *42*).

For a thiol-containing enzyme, one prediction of a reverse protonation mechanism is that an inverse SIE will be apparent on k_{cat}/K_m. This is the case because the fractionation factor of a thiol in D_2O is ~0.5, which results in an up to 2-fold increase in the concentration of the reactive thiolate in D_2O (*35*). Given that the magnitudes of these inverse SIEs on k_{cat}/K_m are similar to the fractionation factor of a thiol in D_2O, these data suggest that the higher rate likely reflects an equilibrium proton transfer to solvent that generates a higher fraction of the more reactive thiolate. Note that similar inverse SIEs on k_{cat}/K_m have been observed for other active site thiol-containing enzymes, including the guanidinium-modifying enzymes PADs 1 and 4 (*28*, *29*) as well as papain (*36*). In contrast, for a pure substrate-assisted mechanism, a normal SIE would be expected because binding to the thiol form of the enzyme is obligatory; thus, the lower concentration of the thiol in D_2O would be expected to have no effect or to decrease k_{cat}/K_m.

To further differentiate between a reverse protonation mechanism and a substrate-assisted mechanism, we evaluated whether the positively charged nature of 2-chloroacetamidine could depress the pK_a of the active site cysteine by mimicking the effect of the positively charged guanidinium group in agmatine.

The results of these studies indicate that the positive charge has an only modest influence on the pK_a of the active site Cys; the pK_a values obtained with 2-chloroacetamidine (9.8 and 8.8) are similar to those obtained (9.2 and 9.6) with iodoacetamide for HpAgD and SmAgD, respectively. Although it is unclear how well 2-chloroacetamidine mimics a true substrate, the fact that this positively charged inactivator does not markedly depress the measured pK_a values further argues against the obligatory binding of the inactivators, and by extension the substrate, to the thiol form of the enzyme as would occur in a "pure" substrate-assisted mechanism (Scheme 1).

Given that the rates of 2-chloroacetamidine inactivation for HpAgD displayed saturable kinetics, it was also possible to obtain a pK_a value from the k_{inact} versus pH rate profile (the measured pK_a is 9.3). The fact that this pK_a is similar to the value obtained from the k_{inact}/K_I versus pH rate profile (i.e., 9.3 and 9.8, respectively) indicates that the positive charge of the inactivator only modestly depresses the pK_a of the active site Cys. As such, these data are also inconsistent with the pure substrate-assisted mechanism because the kinetically preferred pathway suggests that thiolate deprotonation from the reactive species is not required for catalysis.

CONCLUSIONS

pH rate profiles, pK_a inactivation, and solvent isotope experiments suggest that, like the PADs, the AgDs preferentially utilize a reverse protonation mechanism, and not a pure substrate-assisted mechanism. These studies will undoubtedly aid our future efforts to develop inhibitors targeting the AgDs.

REFERENCES

1. Linsky, T., and Fast, W. (2010) Mechanistic similarity and diversity among the guanidine-modifying members of the pentein superfamily. *Biochim. Biophys. Acta 1804*, 1943–1953.
2. Shalev-Alon, G., Sukenik, A., Livnah, O., Schwarz, R., and Kaplan, A. (2002) A novel gene encoding amidinotransferase in the cylindrospermopsin producing cyanobacterium *Aphanizomenon ovalisporum*. *FEMS Microbiol. Lett. 209*, 87–91.
3. Tran, C. T., Leiper, J. M., and Vallance, P. (2003) The DDAH/ADMA/NOS pathway. *Atheroscler. Suppl. 4*, 33–40.
4. Boger, R. H. (2004) Asymmetric dimethylarginine, an endogenous inhibitor of nitric oxide synthase, explains the "L-arginine paradox" and acts as a novel cardiovascular risk factor. *J. Nutr. 134*, 2842S–2847S (discussion 2853S).
5. Leiper, J., Nandi, M., Torondel, B., Murray-Rust, J., Malaki, M., O'Hara, B., Rossiter, S., Anthony, S., Madhani, M., Selwood, D., Smith, C., Wojciak-Stothard, B., Rudiger, A., Stidwill, R., McDonald, N. Q., and Vallance, P. (2007) Disruption of methylarginine metabolism impairs vascular homeostasis. *Nat. Med. 13*, 198–203.
6. Li, Z., Kulakova, L., Li, L., Galkin, A., Zhao, Z., Nash, T. E., Mariano, P. S., Herzberg, O., and Dunaway-Mariano, D. (2009) Mechanisms of catalysis and inhibition operative in the arginine deiminase from the human pathogen *Giardia lamblia*. *Bioorg. Chem. 37*, 149–161.
7. Glazer, E. S., Piccirillo, M., Albino, V., Di Giacomo, R., Palaia, R., Mastro, A. A., Beneduce, G., Castello, G., De Rosa, V., Petrillo, A., Ascierto, P. A., Curley, S. A., and Izzo, F. (2010) Phase II Study of Pegylated Arginine Deiminase for Nonresectable and Metastatic Hepatocellular Carcinoma. *J. Clin. Oncol. 28*, 2220–2226.
8. Jones, J. E., Causey, C. P., Knuckley, B., Slack-Noyes, J. L., and Thompson, P. R. (2009) Protein arginine deiminase 4 (PAD4): Current understanding and future therapeutic potential. *Curr. Opin. Drug Discovery Dev. 12*, 616–627.
9. Sakakibara, Y., and Yanagisawa, H. (2003) Agmatine deiminase from cucumber seedlings is a mono-specific enzyme: Purification and characteristics. *Protein Expression Purif. 30*, 88–93.
10. Baumann, S., Sander, A., Gurnon, J. R., Yanai-Balser, G. M., Van Etten, J. L., and Piotrowski, M. (2007) Chlorella viruses contain genes encoding a complete polyamine biosynthetic pathway. *Virology 360*, 209–217.
11. Griswold, A. R., Jameson-Lee, M., and Burne, R. A. (2006) Regulation and physiologic significance of the agmatine deiminase system of *Streptococcus mutans* UA159. *J. Bacteriol. 188*, 834–841.
12. Williams, B. J., Du, R. H., Calcutt, M. W., Abdolrasulnia, R., Christman, B. W., and Blackwell, T. S. (2010) Discovery of an operon that participates in agmatine metabolism and regulates biofilm formation in *Pseudomonas aeruginosa*. *Mol. Microbiol. 76*, 104–119.
13. Li, G., Regunathan, S., Barrow, C. J., Eshraghi, J., Cooper, R., and Reis, D. J. (1994) Agmatine: An endogenous clonidine-displacing substance in the brain. *Science 263*, 966–969.
14. Regunathan, S., and Reis, D. J. (1996) Imidazoline receptors and their endogenous ligands. *Annu. Rev. Pharmacol. Toxicol. 36*, 511–544.
15. Satriano, J. (2004) Arginine pathways and the inflammatory response: Interregulation of nitric oxide and polyamines: Review article. *Amino Acids 26*, 321–329.
16. Joshi, M. S., Ferguson, T. B., Jr., Johnson, F. K., Johnson, R. A., Parthasarathy, S., and Lancaster, J. R., Jr. (2007) Receptor-mediated activation of nitric oxide synthesis by arginine in endothelial cells. *Proc. Natl. Acad. Sci. U.S.A. 104*, 9982–9987.
17. Su, C. H., Liu, I. M., Chung, H. H., and Cheng, J. T. (2009) Activation of I2-imidazoline receptors by agmatine improved insulin sensitivity through two mechanisms in type-2 diabetic rats. *Neurosci. Lett. 457*, 125–128.
18. Gobert, A. P., McGee, D. J., Akhtar, M., Mendz, G. L., Newton, J. C., Cheng, Y., Mobley, H. L., and Wilson, K. T. (2001) *Helicobacter pylori* arginase inhibits nitric oxide production by eukaryotic cells: A strategy for bacterial survival. *Proc. Natl. Acad. Sci. U.S.A. 98*, 13844–13849.
19. Jones, J. E., Causey, C. P., Lovelace, L., Knuckley, B., Flick, H., Lebioda, L., and Thompson, P. R. (2010) Characterization and inactivation of an agmatine deiminase from *Helicobacter pylori*. *Bioorg. Chem. 38*, 62–73.
20. Luo, Y., Arita, K., Bhatia, M., Knuckley, B., Lee, Y. H., Stallcup, M. R., Sato, M., and Thompson, P. R. (2006) Inhibitors and inactivators of protein arginine deiminase 4: Functional and structural characterization. *Biochemistry 45*, 11727–11736.
21. Luo, Y., Knuckley, B., Lee, Y. H., Stallcup, M. R., and Thompson, P. R. (2006) A fluoroacetamidine-based inactivator of protein arginine deiminase 4: Design, synthesis, and in vitro and in vivo evaluation. *J. Am. Chem. Soc. 128*, 1092–1093.
22. Luo, Y., Knuckley, B., Bhatia, M., Pellechia, P. J., and Thompson, P. R. (2006) Activity-based protein profiling reagents for protein arginine deiminase 4 (PAD4): Synthesis and in vitro evaluation of a fluorescently labeled probe. *J. Am. Chem. Soc. 128*, 14468–14469.
23. Causey, C. P., and Thompson, P. R. (2008) An improved synthesis of haloaceteamidine-based inactivators of protein arginine deiminase 4 (PAD4). *Tetrahedron Lett. 49*, 4383–4385.
24. Stone, E. M., Schaller, T. H., Bianchi, H., Person, M. D., and Fast, W. (2005) Inactivation of two diverse enzymes in the amidinotransferase superfamily by 2-chloroacetamidine: Dimethylargininase and peptidylarginine deiminase. *Biochemistry 44*, 13744–13752.
25. Wang, Y., Hu, S., and Fast, W. (2009) A click chemistry mediated in vivo activity probe for dimethylarginine dimethylaminohydrolase. *J. Am. Chem. Soc. 131*, 15096–15097.
26. Li, L., Li, Z., Chen, D., Lu, X., Feng, X., Wright, E. C., Solberg, N. O., Dunaway-Mariano, D., Mariano, P. S., Galkin, A., Kulakova, L., Herzberg, O., Green-Church, K. B., and Zhang, L. (2008) Inactivation of microbial arginine deiminases by L-canavanine. *J. Am. Chem. Soc. 130*, 1918–1931.
27. Stone, E. M., Costello, A. L., Tierney, D. L., and Fast, W. (2006) Substrate-assisted cysteine deprotonation in the mechanism of dimethylargininase (DDAH) from *Pseudomonas aeruginosa*. *Biochemistry 45*, 5618–5630.
28. Knuckley, B., Bhatia, M., and Thompson, P. R. (2007) Protein arginine deiminase 4: Evidence for a reverse protonation mechanism. *Biochemistry 46*, 6578–6587.
29. Knuckley, B., Causey, C. P., Jones, J. E., Bhatia, M., Dreyton, C. J., Osborne, T. C., Takahara, H., and Thompson, P. R. (2010) Substrate specificity and kinetic studies of PADs 1, 3, and 4 identify potent and selective inhibitors of protein arginine deiminase 3. *Biochemistry 49*, 4852–4863.
30. Griswold, A. R., Nascimento, M. M., and Burne, R. A. (2009) Distribution, regulation and role of the agmatine deiminase system in mutans streptococci. *Oral Microbiol. Immunol. 24*, 79–82.
31. Kearney, P. L., Bhatia, M., Jones, N. G., Yuan, L., Glascock, M. C., Catchings, K. L., Yamada, M., and Thompson, P. R. (2005) Kinetic characterization of protein arginine deiminase 4: A transcriptional

corepressor implicated in the onset and progression of rheumatoid arthritis. *Biochemistry 44*, 10570–10582.
32. Knipp, M., and Vasak, M. (2000) A colorimetric 96-well microtiter plate assay for the determination of enzymatically formed citrulline. *Anal. Biochem. 286*, 257–264.
33. Leatherbarrow, R. J. (2004) GraFit, version 5.0, Erathicus Software, Staines, U.K.
34. Karsten, W. E., Lai, C. J., and Cook, P. F. (1995) Inverse Solvent Isotope Effects in the Nad-Malic Enzyme Reaction Are the Result of the Viscosity Difference between D_2O and H_2O: Implications for Solvent Isotope Effect Studies. *J. Am. Chem. Soc. 117*, 5914–5918.
35. Quinn, D. M., and Sutton, L. D. (1991) Theoretical basis and mechanistic utility of solvent isotope effects. In Enzyme Mechanism from Isotope Effects (Cook, P. F., Ed.) pp 73−126, CRC Press, Boca Raton, FL.
36. Lewis, S. D., Johnson, F. A., and Shafer, J. A. (1981) Effect of cysteine-25 on the ionization of histidine-159 in papain as determined by proton nuclear magnetic resonance spectroscopy. Evidence for a His-159−Cys-25 ion pair and its possible role in catalysis. *Biochemistry 20*, 48–51.
37. Knuckley, B., Causey, C. P., Pellechia, P. J., Cook, P. F., and Thompson, P. R. (2010) Haloacetamidine-based inactivators of protein arginine deiminase 4 (PAD4): Evidence that general acid catalysis promotes efficient inactivation. *ChemBioChem 11*, 161–165.
38. Galkin, A., Lu, X., Dunaway-Mariano, D., and Herzberg, O. (2005) Crystal structures representing the Michaelis complex and the thiouronium reaction intermediate of *Pseudomonas aeruginosa* arginine deiminase. *J. Biol. Chem. 280*, 34080–34087.
39. Ke, Z., Wang, S., Xie, D., and Zhang, Y. (2009) Born-Oppenheimer ab initio QM/MM molecular dynamics simulations of the hydrolysis reaction catalyzed by protein arginine deiminase 4. *J. Phys. Chem. B 113*, 16705–16710.
40. Ke, Z., Zhou, Y., Hu, P., Wang, S., Xie, D., and Zhang, Y. (2009) Active site cysteine is protonated in the PAD4 Michaelis complex: Evidence from Born-Oppenheimer ab initio QM/MM molecular dynamics simulations. *J. Phys. Chem. B 113*, 12750–12758.
41. Frankel, B. A., Kruger, R. G., Robinson, D. E., Kelleher, N. L., and McCafferty, D. G. (2005) *Staphylococcus aureus* sortase transpeptidase SrtA: Insight into the kinetic mechanism and evidence for a reverse protonation catalytic mechanism. *Biochemistry 44*, 11188–11200.
42. Mock, W. L., and Stanford, D. J. (2002) Anisylazoformylarginine: A superior assay substrate for carboxypeptidase B type enzymes. *Bioorg. Med. Chem. Lett. 12*, 1193–1194.